Journal of Wind Engineering and Industrial Aerodynamics, 39 (1992) 105–118
Elsevier Science Publishers B.V., Amsterdam — Printed in The Netherlands

Static pressure measurements on a rotating and a non-rotating 2.375 m wind turbine blade. Comparison with 2D calculations

Göran Ronsten

FFA, The Aeronautical Research Institute of Sweden, Box 11021, S-161 11 Bromma, Sweden

Summary

Static pressure distributions on a 5.35 m diameter, horizontal axis wind turbine have been measured in the CARDC (China Aerodynamic Research and Development Centre) low speed wind tunnel. The pressure distributions on one of the two blades have also been recorded during non-rotating operation in the FFA-LT1 low speed wind tunnel.

By applying the Lanchester-Prandtl lifting line theory, 2D equivalent angles of attack (AOA) for the non-rotating blade (NRB) were calculated for each radial station. Using XFOIL, a 2D airfoil analysis code, pressure distributions were calculated at the 2D AOA from lifting line calculations. The XFOIL pressure distributions were compared with data for the NRB. Good agreement was found, especially at Re numbers exceeding 500 000 at all radial stations but for $r/R=99\%$.

In order to attain the local AOA at each radial station on the rotating blade (RB), the pressure distributions on the RB were compared with data from the NRB. It is assumed, at AOA below stall, that when the pressure signature around the stagnation point is equal for both the RB and the NRB, then the AOA is the same.

Significant differences in $C_l(\alpha)$ between the RB and the NRB were found only at $r/R=30\%$. At $r/R=30\%$, no drop in C_l could be measured on the RB even at high AOA, where the NRB since long had stalled.

Derived $C_l(\alpha)$ and $C_d(\alpha)$ for the NRB were used as input to WINRO, a computer program based on blade element/momentum theory (BEM). The RB tip seems to be more lightly loaded than predicted by WINRO at all tip speed ratios.

Symbols

A	πR^2	disc area [m^2]
a	$(V-U)/V$	axial induction
a'	ω/Ω	angular induction
c		local chord [m]
C_d	d/cq_w	drag coefficient
C_l	l/cq_w	lift coefficient
C_p	$1+(p-p_0)/q_w$	pressure coef.
C_P	P/AVq_v	power coef.

C_T	T/q_v	thrust force coef.
C_x	x/cq_w	tangent. force coef.
C_y	y/cq_w	normal force coef.
d		drag force (2D) [N]
l		lift force (2D) [N]
P		power [N m/s]
p		blade surface pressure [N/m^2]
p_0		stagnation pressure [N/m^2]
q_w	$0.5\rho W^2$	dynamic pressure [N/m^2]
q_v	$0.5\rho V^2$	dynamic pressure [N/m^2]
R		blade radius [m]
r		local radius [m]
s		airfoil arc length [m]
T		thrust force [N]
U		axial wind speed, disc [m/s]
V		Wind speed, upstream [m/s]
W	$\sqrt{[V(1-a)]^2+[r\omega(1+a')]^2}$	local inflow velocity [m/s]
V_{hel}	$\sqrt{V^2+(r\omega)^2}$	helical velocity [m/s]
v		blade surface velocity [m/s]
x		tangential force, airfoil [N]
y		normal force, airfoil [N]
α		angle of attack [deg]
λ	$R\omega/V$	tip speed ratio
λ_r	$r\omega/V$	local tip speed ratio
ρ		density [kg/m^2]
Ω		rotor angular velocity [rad/s]
ω		angular velocity [rad/s]

Abbreviations

AOA	angle of attack. For the NRB, the geometric AOA=pitch minus twist
BEM	blade element/momentum theory
CARDC	China Aerodynamic Research and Development Centre
FFA	The Aeronautical Research Institute of Sweden
LLC	lifting line calculations
NRB	non-rotating blade
RB	rotating blade
TSR	tip speed ratio
WINRO	BEM-based computer code at FFA
XFOIL	2D airfoil analysis computer code

1. Introduction

The power from a wind turbine normally exceeds the calculated power using BEM methods. The relevance of tip loss correction factors being used in BEM

methods and the relation between induced velocity and thrust need to be investigated in order to make it possible to modify the BEM calculation models used in WINRO [1].

2. The non-rotating blade

Pressure distributions were measured on a conventional STORK 5WPX blade equipped with a total of 232 pressure taps at 8 radial stations (Fig. 1). *The blade geometries at each radial station were measured at the FFA workshop after the pressure taps had been installed.* General data for the blade were presented in [2].

2.1. Static pressure measurements

A Scanivalve unit with five transducers mounted in parallel was used to acquire blade surface pressures. 30 data points were collected for each pressure

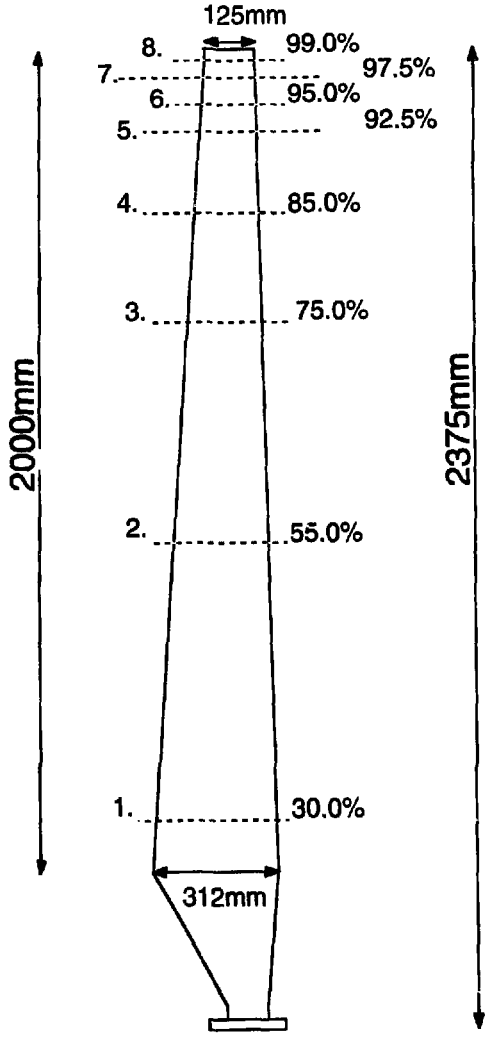

Fig. 1. Radial location of pressure tap stations.

tap. As the tubing was up to 3 m long, only the average pressures were used in the calculations.

2.2. Integrated pressure distributions

A resulting force and its direction were calculated using linear interpolation between the measured pressures at each radial station. A cubic spline was applied in the radial direction between the pressure tap stations when calculating the flap and edge moments at the blade root. These moments were also measured using a blade root bending moment balance. The agreement between the flap- and edge-wise bending moments is good, Fig. 2.

2.3. Equivalent 2D AOA

The Lanchester–Prandtl lifting line theory [4] was used in order to obtain the 2D equivalent angle of attack and thus the "2D" $C_l(\alpha)$ relation. The bound vorticity was assumed to be zero at the tip and at 15% radius. The radial distribution of circulation can be calculated by applying the Kutta–Joukowsky relation:

$$\Gamma = l/\rho V. \tag{1}$$

As a first approximation, the geometric AOA was used for calculating the lift force from the measured normal and tangential forces. Convergence was achieved after 10 to 20 iterations with the criteria that the AOA at any radial station should not differ by more than 1/100 of a degree between successive runs. (This is not claimed to be the accuracy of the method.)

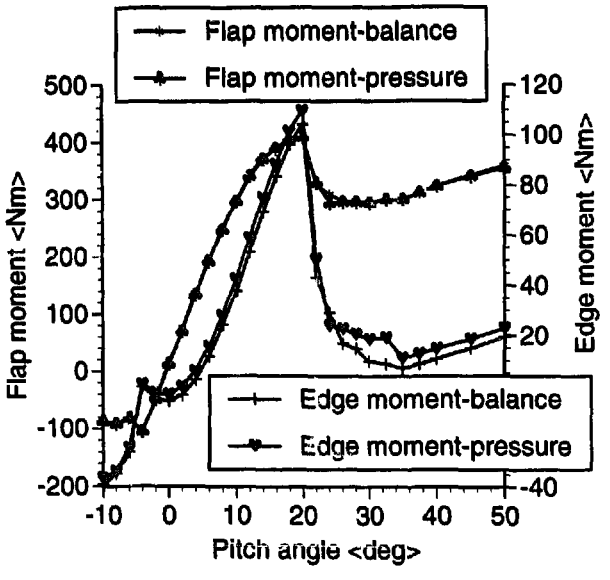

Fig. 2. Blade root bending moments, NRB, from balance and integrated pressure distributions at $V = 30$ m/s.

2.4. 2D airfoil calculations - XFOIL

A 2D airfoil analysis computer program, XFOIL, a derivative of ISES, [5], was used to compare the $C_l(\alpha)$ relationship from lifting line calculations (LLC) with theoretical calculations. In Fig. 3, $C_l(\alpha)$ for the radial position $r/R=75\%$ at Re = 720 000, is compared with C_l from XFOIL.

2.5. Massive separation or radial flow on the NRB

An alternative to the Kutta–Joukowsky expression for the circulation (1) can be utilized:

$$\Gamma=\oint(\bar{v})\,\mathrm{d}\bar{s} \tag{2}$$

Eq. (2) is applicable when the flow is attached and directed in the chordwise direction. The blade surface velocities are calculated by applying Bernoulli's theorem to the measured pressures.

$C_l(\alpha)$ from Eq. (2) is compared to $C_l(\alpha)$ from LLC. If C_l is allowed to differ no more than, for example, 5% at the same AOA (from LLC), then an AOA versus radius where radial flow and/or massive separation occurs can be shown, Fig. 4.

2.6. Pressure distributions - NRB and XFOIL

A data base with C_p versus AOA and arc length along each airfoil was made up using XFOIL. The calculations covered the same Re number region as the wind tunnel data. The C_p distribution for one such case can be seen in Fig. 5, AOA is from LLC.

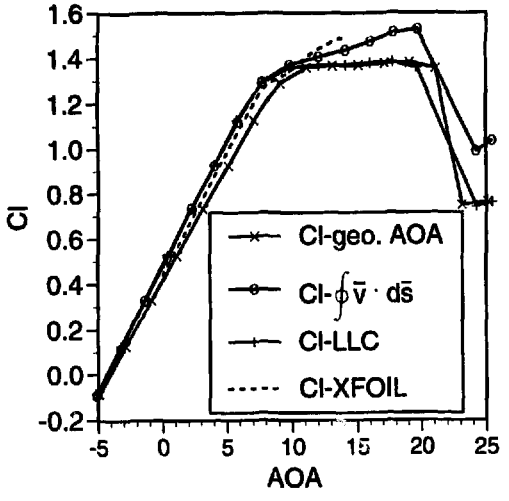

Fig. 3. $C_l(\alpha)$ for different calculational methods at $r/R=75\%$, Re = 720 000.

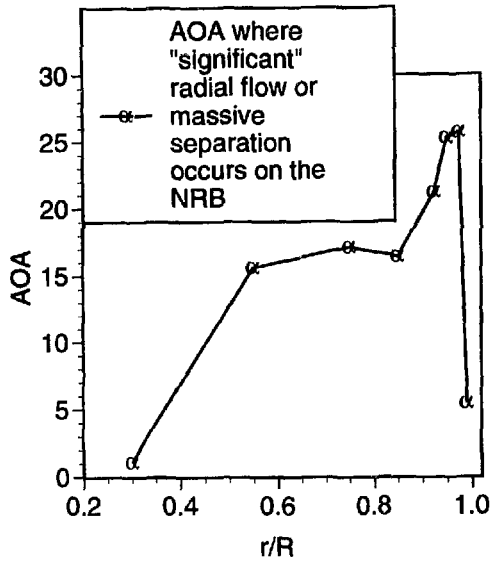

Fig. 4. AOA where $C_l(\alpha)$ from LLC and $C_l(\alpha)$ from Eq. (2), differ by more than 5%. $V=55$ m/s.

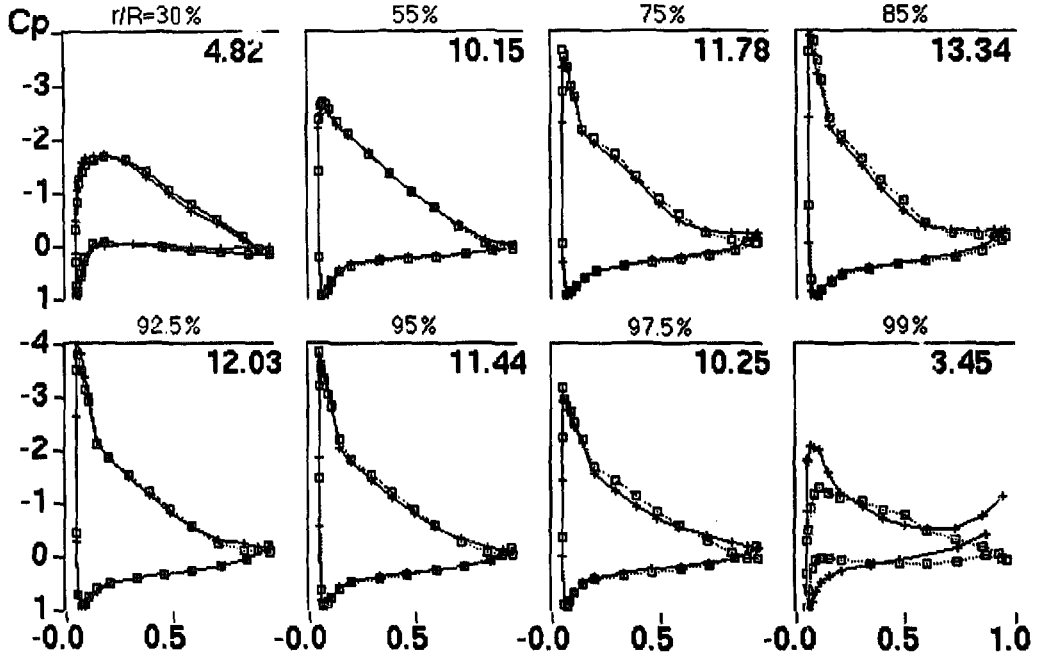

Fig. 5. C_p distribution for the NRB (crosses) compared to XFOIL (squares) at AOA from LLC. Pitch=16°, $V=55$ m/s.

3. The rotating blade

The rotating test rig and the general characteristics of the CARDC low speed wind tunnel were presented in [2]. Wind tunnel blockage was taken into account through the use of the "Wall Pressure Signature Matrix Method" [3]. Centrifugal forces were corrected for using methods presented in [8].

3.1. AOA for the RB sections

The pressure distribution below apex for each airfoil on the RB was compared, through an iterative process, to the NRB data bank with pressure distributions at different AOA and Re numbers. Starting at a certain geometric AOA for the expression

$$\sum |C_{P_{RB}}(s_i) - C_{P_{NRB}}(\alpha, s_i)|. \tag{3}$$

The estimated geometric AOA at the minima, was then translated into an equivalent 2D AOA. This was done through linear interpolation in the relationship from LLC between the geometric AOA and the 2D equivalent AOA.

This 2D equivalent AOA was used to calculate the local inflow velocity, W, and thus a new dynamic pressure for the RB airfoil section. The rescaled C_p-distribution from the RB was then used as input to Eq. (3). It took between 2 and 4 iterations before the solution had converged to within 1/100 of a degree (which is not the accuracy of this method).

The locations and the number of pressure taps included in the summation were chosen after examining the $C_p(\alpha)$ relationship for each pressure tap location. The five pressure taps located below the leading edge were selected and an example of the influence of the number of pressure taps included in Eq. (3) is shown in Fig. 6. A series of corresponding pressure distributions can be seen in Fig. 7.

When the calculated AOA was higher than 16° (20° at $r/R=30\%$), the geometrical AOA from LLC was set equal to the AOA that would be if there was no induction on the RB. This is a crude estimate that could be replaced by for example Glauert's relationship between axial induction and trust force, used in BEM theory.

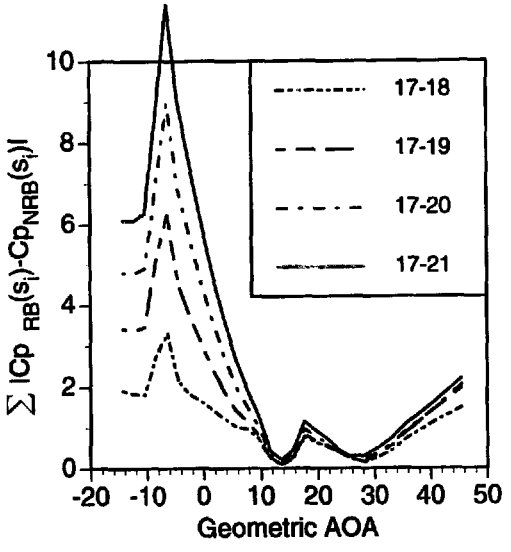

Fig. 6. Influence of the number of pressure taps included in (3). Tap No. 16 is close to the leading edge. Increasing numbers on the pressure side.

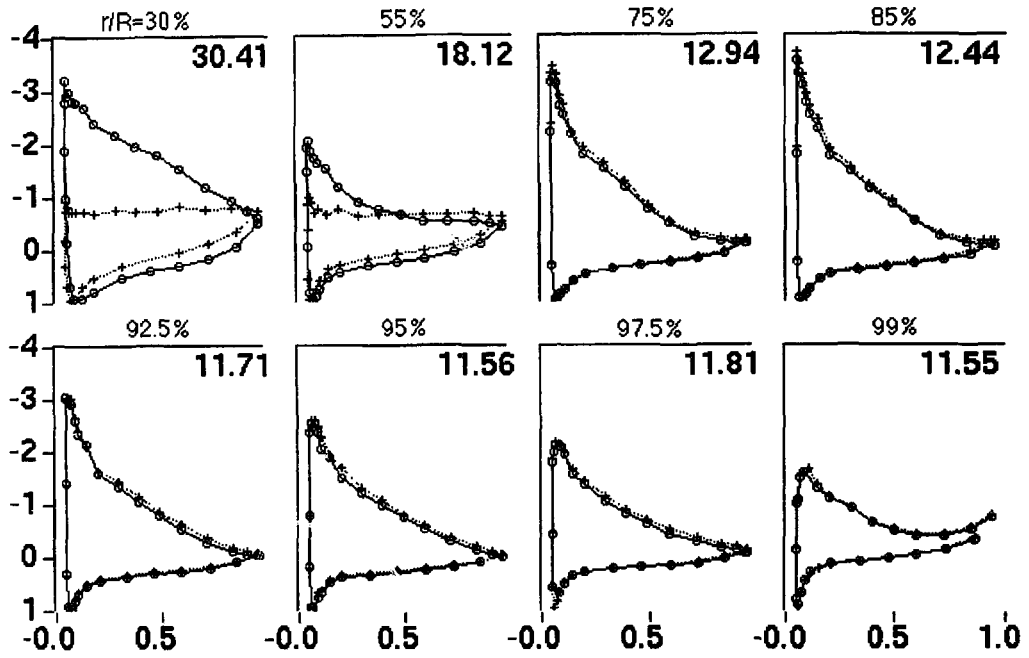

Fig. 7. Corresponding pressure distributions for the RB (circle) and the NRB (cross) at $\lambda = 4.32$. AOA (upper right corner) from LLC.

3.2. *WINRO*

WINRO, a computer program based on BEM theory [1], is used at FFA to calculate the performance of HAWTs. Three-dimensional effects are not accounted for except at the tip and the root where a method by Prandtl [6] is applied.

Calculations with WINRO were carried out with aerodynamic data from the NRB. Skin friction was approximated by adding $\Delta C_d = 0.008$ to the pressure drag. The Prandtl tip and hub loss factor were used for all calculations.

Two different $C_T(a)$ models were applied:

(1) The standard Glauert model.

(2) A $C_T(a)$ model, MOMEXT, made up by Meijer (FFA) after comparisons with more time consuming vortex program calculations.

Calculations were also carried by using the Wilson axial induction interference model [8].

For one series of calculations, the aerodynamic data for $r/R = 55\%$ and 75% were used at the out- and inward stations respectively. $C_P(\lambda)$ for the different calculation models at a pitch angle of 0° are shown in Fig. 8. The power coefficient for the rotating case is calculated using the torque from the six-component strain gauge balance used during the CARDC test on the rotating turbine. Pressure distributions from XFOIL, at the AOA calculated by WINRO using the Glauert $C_T(a)$, are compared with data from the RB in Fig. 9.

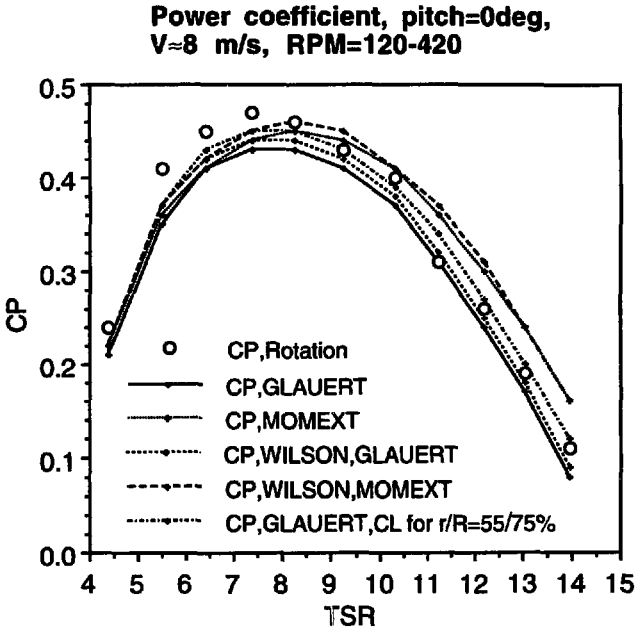

Fig. 8. Power coefficient versus tip speed ratio with different calculation models.

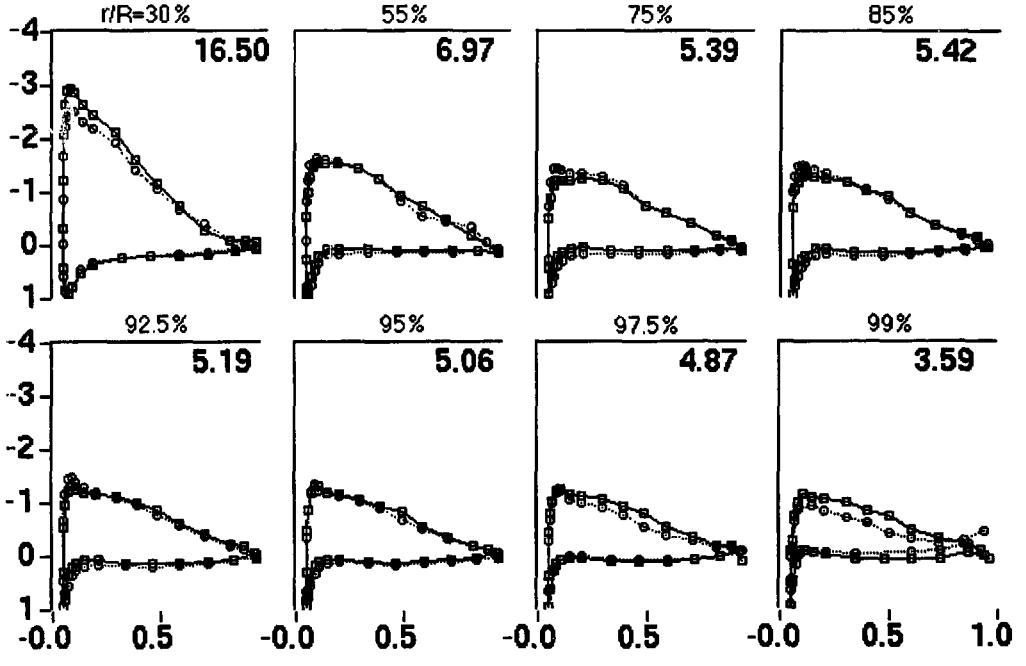

Fig. 9. C_p at TSR 7.37. Squares represent XFOIL calculations and circles data from the RB. AOA from WINRO.

3.3. $C_l(\alpha)$ for the RB and the NRB

Figures 10–12 show $C_l(\alpha)$ at $r/R=30\%$, 55% and 97.5% for the RB and the NRB for all Re numbers covered. Only at 30% radius did C_l not decrease even at the lowest TSR ($\lambda=3.72$). A slightly lower C_l at the tip at the corresponding

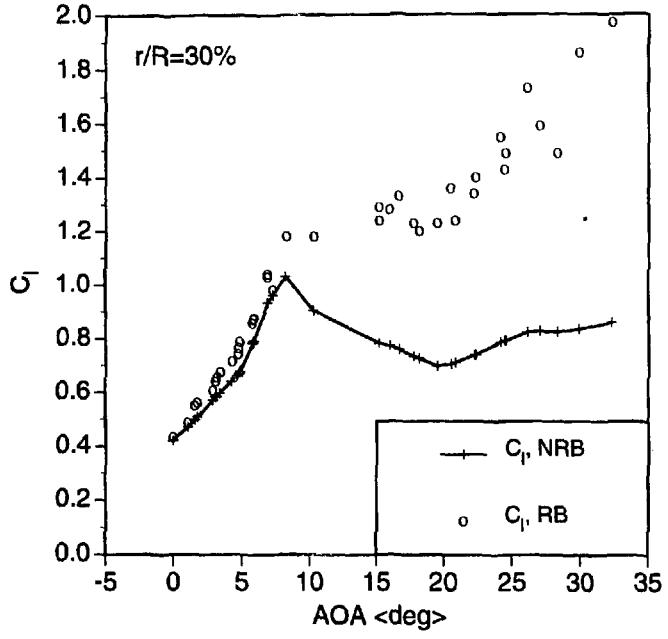

Fig. 10. $C_l(\alpha)$ for the NRB and the RB at $r/R=30\%$.

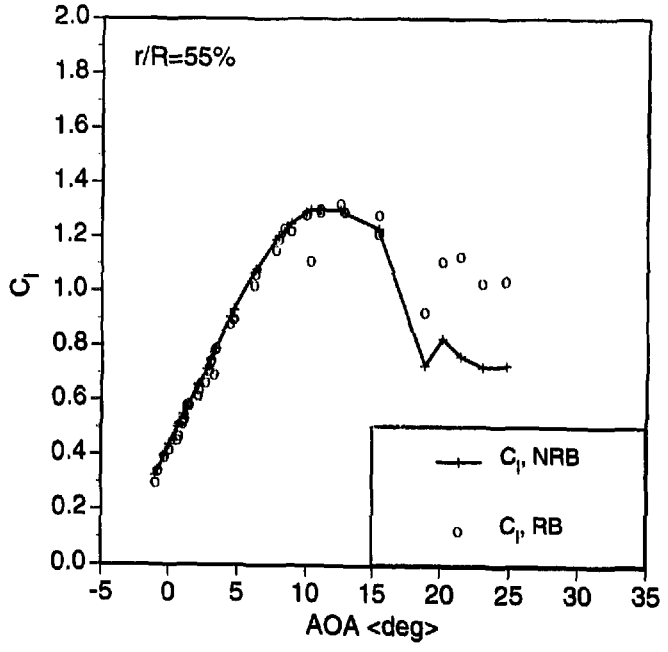

Fig. 11. $C_l(\alpha)$ for the NRB and the RB at $r/R=55\%$.

AOA from eq. (3) was the output from this comparison. It should be noted that the Re number at the tip reached above 1 million on the RB while it only reached 500 000 on the NRB.

3.4. $C_x(\lambda,r)$ for the RB

Figure 13 shows $C_x(\lambda,r)$ for the RB.

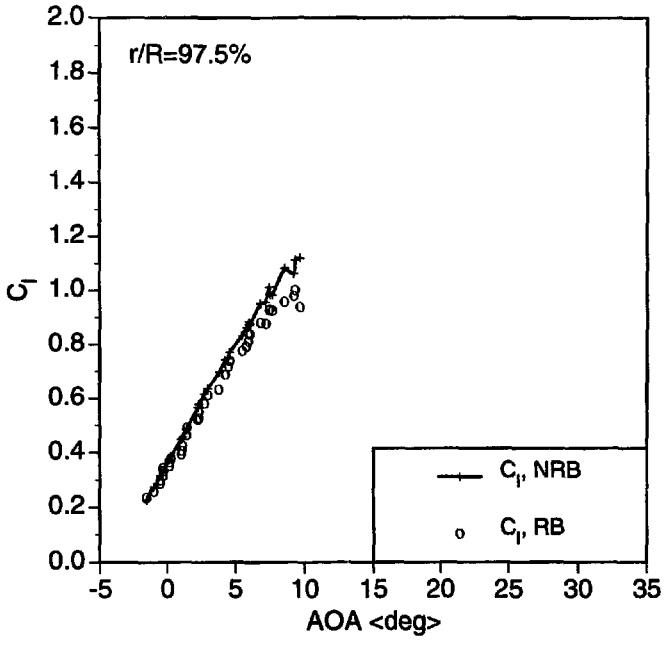

Fig. 12. $C_l(\alpha)$ for the NRB and the RB at r/R=97.5%.

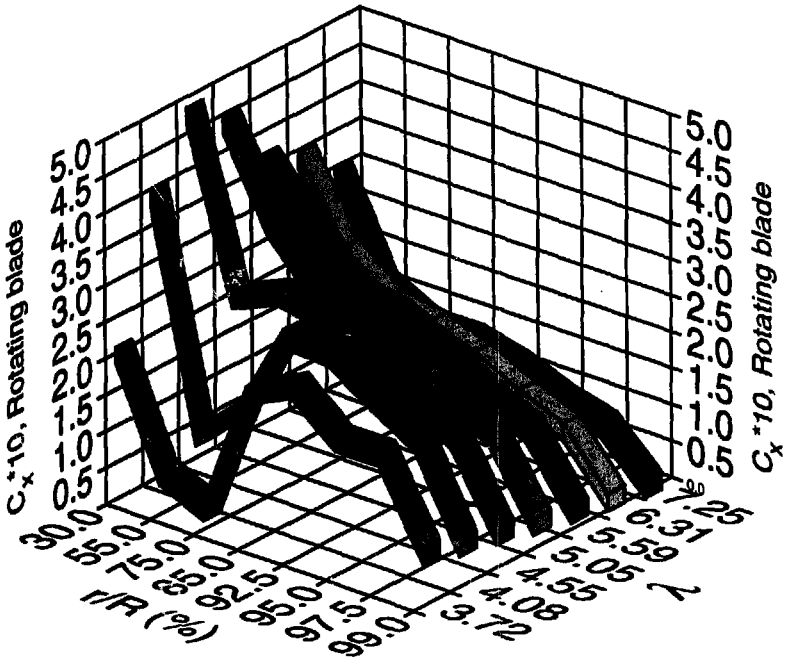

Fig. 13. $C_x(\lambda,r)$ for the RB.

3.5. $dC_x(\lambda,r)$ for the RB and the NRB

Figure 14 shows the difference between $C_x(\lambda,r)$ for the RB and $C_x(\lambda,r)$ calculated using WINRO with the Glauert $C_T(a)$ model.

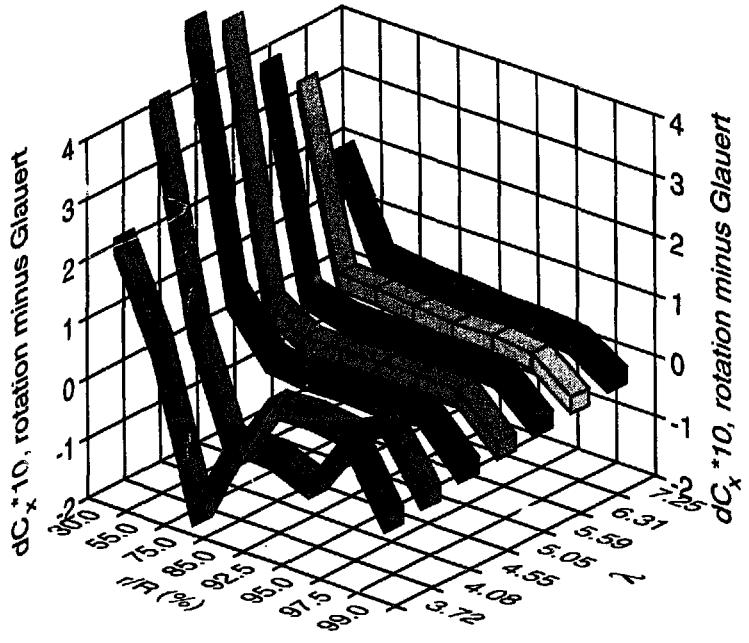

Fig. 14. $dC_x(\lambda,r) = C_x$ for the RB minus C_x for the NRB calculated using WINRO (Glauert).

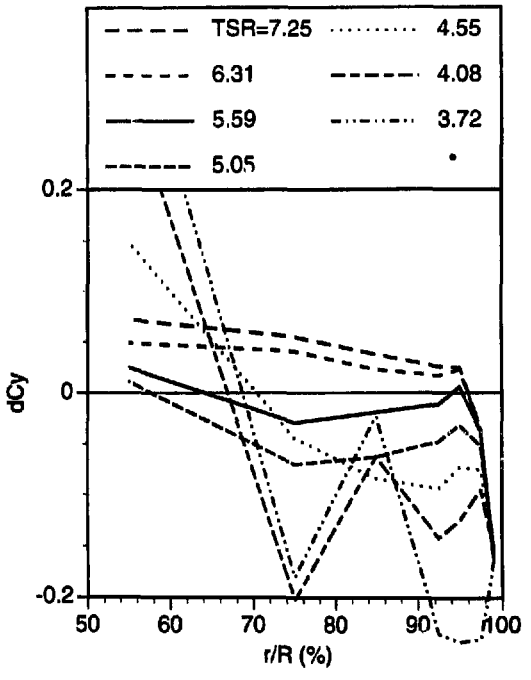

Fig. 15. $dC_y(\lambda,r) = C_y$ for the RB minus C_y calculated using WINRO with the Glauert $C_T(a)$ relation and the Prandtl tip correction factor.

3.6. $dC_y(\lambda,r)$ for the RB and the NRB

Figure 15 shows the difference between $C_y(\lambda,r)$ for the RB and $C_y(\lambda,r)$ calculated using WINRO with the Gluert $C_T(a)$ model.

4. Results

4.1. 2D $C_l(\alpha)$

Comparing calculated $C_l(\alpha)$ from XFOIL and $C_l(\alpha)$ from the non-rotating blade with the local 2D AOA from the Prandtl–Lanchester lifting line theory indicates that the theory produces good estimates for the 2D equivalent angle of attack for a wind turbine blade, equipped with pressure taps, under non-rotating conditions.

4.2. Rotational effects

A 2D equivalent angle of attack was calculated for the rotating blade section. Good agreement was found between $C_l(\alpha)$ for the rotating and the non-rotating blade up to moderate angles of attack at all radial stations. $C_l(\alpha)$ at the innermost radial station did not decrease at high angles of attack on the rotating blade as it did on the non-rotating blade.

4.3. Pressure distributions

The Prandtl tip correction factor does not off-load the tip as much as is needed in order to obtain good correlation between calculations and measurements.

The hub region experiences higher loadings at low tip speed ratios than is predicted when using 2D data. This, so called Himmelskamp effect, delays the stall at the root. At high angles of attack a triangular shaped pressure distribution seems typical close to the root during rotation. The stall on the middle part of the blade, in the radial direction, occurs at a higher TSR than WINRO predicts.

4.4. Power

At low to medium TSR the power is underpredicted by WINRO, using the Glauert $C_T(a)$, when compared to the measured mechanical torque. At high tip speed ratios the agreement is better.

5. Concluding remarks

The results are especially sensitive to the tunnel blockage corrections at high TSR. As the magnitude of the correction is smaller for low TSR than for high TSR, the results are therefore more reliable at low TSR.

However, at low TSR, the difficulty in finding an equivalent AOA increases. A method for determining the instantaneous AOA from examination of a pressure distribution would be appreciated.

Acknowledgements

This work has been funded by the National Swedish Energy Administration. Anders Björck at FFA carried out the XFOIL calculations.

References

1 A.L. Gustafsson, S. Lundgren and B. Frisk, Application of a Method for Aerodynamic Analysis and Design of Horizontal Axis Wind Turbines, FFA 1980.
2 G. Ronsten, J.A. Dahlberg and S. Meijer, Pressure measurements on a 5.35 m HAWT in CARDC 12×16 m wind tunnel compared to theoretical pressure distributions, EWEC '89, European Wind Energy Conference and Exhibition. Glasgow, Scotland.
3 He Dexin and Jiang Guiqing, An investigation of blockage corrections for wind turbine tests in CARDC low speed wind tunnel, CARDC-86-1020, 1986.
4 Duncan, Thom and Young, Mechanics of Fluids (Arnold, London, 1970).
5 M. Drela and M.B. Giles, Viscous-invicsid analysis of transonic and low Reynolds number airfoils, AIAA J., 25(10) (1988) 1347-1355.
6 R.M. Bass, Small scale wind tunnel testing of model propellers, AIAA 24th Aerospace Sciences Meeting, January 6-9, 1986, Reno, Nevada.
7 H. Glauert, The analysis of experimental results in the windmill brake and vortex ring state of an airscrew, R&M No. 1026 AE 22, 1926.
8 R.E. Wilson, P.B.S. Lissaman and S.N. Walker, Aerodynamic Performance of Wind Turbines, Oregon State University, June 1976.